Yii-Mei Huang
Chih-Shan Hsu
Department of Mechanical Engineering
National Central University
Chung-Li, Taiwan, 320
Republic of China
E-mail:
T330005@sparc20.ncu.edu.tw

Dynamic Behavior of Tubes Subjected to Internal and External Cross Flows

This article presents a method for thoroughly examining the dynamic characteristics of a tube under the influence of either the internal flow or the external cross flow. The tube is modeled as a thin cylindrical shell whose governing equations are derived from an energy method. The effects due to internal flow are introduced into the system through initial stress. Galerkin's method in conjunction with the method of multiple scales is employed for obtaining the stability of the tube vibration. According to the results, instability can occur under certain conditions of resonance. Regarding the effects of the external cross flow, a numerical approach is initially employed to interpolate the experimental data of the pressure distributions due to the flow. The dynamic characteristics of the tube under steady flows and flows with small time variation are then investigated. Stability of the solution is also discussed. © *1997 John Wiley & Sons, Inc.*

INTRODUCTION

Shell-type structures have been extensively used in constructional, mechanical, and many other applications, e.g., pressure vessels, heat exchanger tubes, etc. Hence the dynamic effects arising from the interactions of internal flows and external cross flows are of interest. Most literature concentrated on identifying critical flow velocity (Blevins, 1977; Chen, 1987). The flow effects on dynamic behaviors of tubes, although important, are not discussed intensively. This article examines the shell's vibration and its stability and serves as a preliminary study of the dynamic behavior of a tube under the influence of internal/external cross flows.

This study employs thin shell theory for the tube. Huang and Hsu (1990) once derived the spinning thin shell equations, in which the initial stresses caused by rotation was included. Weaver and Unny (1973) used the Flugge–Kempner cylindrical shell equations and the potential flow theory to describe the dynamic pressure of internal flows, and they also discussed the stability phenomena. Yao (1963) employed the Donell–Vlasov equations and more thoroughly examined the instability under the action of radial and longitudinal loadings. The current research adopts the theory of Huang and Hsu (1990), modifying it such that the pressure due to the flow is included as the initial stress. The variance of the natural frequencies of the shell with system parameters is then discussed. Moreover, instability resulting from small time variation of the flow is also investigated.

Received October 20, 1995; Accepted October 17, 1996

Shock and Vibration, Vol. 4, No. 2, pp. 77–91 (1997)

CCC 1070-9622/97/020077-15

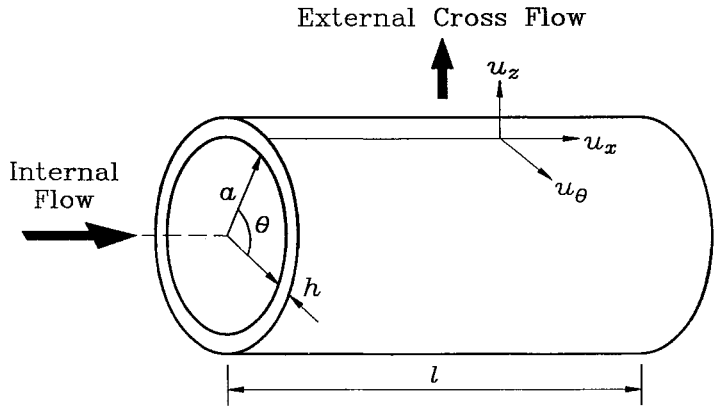

FIGURE 1 The cylindrical shell model for a tube subjected to internal and external cross flows.

EQUATIONS OF MOTION

Figure 1 depicts a cylindrical tube excited by an internal flow or an external cross flow. This article attempts to develop a relatively simple technique of analyzing the dynamics of the tube without involving complicated fluid dynamics. We consider the initial circumferential stress caused by the flow. The initial stress σ^i is of the form

$$\sigma^i = \frac{a}{h} \cdot p, \tag{1}$$

where p represents the pressure generated by the internal or the external cross flow and a and h denote the mean radius and thickness of the tube, respectively. By employing Hamilton's principle, the equations of motion of the cylindrical shell subjected to the flow are then derived as

$$\{[L_L] + [L_P]\}\mathbf{u} = \mathbf{0}, \tag{2}$$

where

$$[L_L] = \begin{bmatrix} \left[\frac{K}{l^2}\frac{\partial^2}{\partial\xi^2} + \frac{K(1-\nu)}{2a^2}\frac{\partial^2}{\partial\theta^2} - \rho h\frac{\partial^2}{\partial t^2}\right] & \frac{K(1+\nu)}{2al}\frac{\partial^2}{\partial\xi\partial\theta} & \frac{\nu K}{al}\frac{\partial}{\partial\xi} \\ & \left[\frac{1-\nu}{2l^2}\left(K+\frac{D}{a^2}\right)\frac{\partial^2}{\partial\xi^2} + \left(\frac{D}{a^4}+\frac{K}{a^2}\right)\frac{\partial^2}{\partial\theta^2} - \rho h\frac{\partial^2}{\partial t^2}\right] & \left[-\frac{D}{a^4}\frac{\partial^3}{\partial\theta^3} + \frac{K}{a^2}\frac{\partial}{\partial\theta} - \frac{D}{a^2l^2}\frac{\partial^3}{\partial\xi^2\partial\theta}\right] \\ \text{sym.} & & \left[\frac{D}{a^4}\nabla^4 + \frac{K}{a^2} + \rho h\frac{\partial^2}{\partial t^2}\right] \end{bmatrix} \tag{3}$$

is the differential operator based on Love–Timoshenko theory (Soedel, 1981), and

$$[L_P] = \begin{bmatrix} \frac{p}{a}\frac{\partial^2}{\partial\theta^2} & 0 & 0 \\ & \left[\frac{p}{a}\frac{\partial^2}{\partial\theta^2} - \frac{p}{a}\right] & 2\frac{p}{a}\frac{\partial}{\partial\theta} \\ \text{sym.} & & \left[\frac{p}{a} - \frac{p}{a}\frac{\partial^2}{\partial\theta^2}\right] \end{bmatrix} \quad (4)$$

is the differential operator resulting from the flow. Notably, both operators are symmetric, thereby ensuring that the eigenvalues of the system are real (Leissa, 1973). In the above equations, $\xi = x/l$ is a dimensionless axial coordinate, ν is the Poisson's ratio, and $\mathbf{u} = \{u_x, u_\theta, u_z\}^T$ denotes the displacement vector. Notation $\nabla^4 = \nabla^2\nabla^2$ is the biharmonic operator, and $\nabla^2 = \partial^2/\partial\theta^2 + (a/l)^2\partial^2/\partial\xi^2$. The membrane stiffness and bending stiffness of the shell are denoted as $K = h/(1 - \nu^2)$ and $D = h^3/[12(1 - \nu^2)]$, respectively. In deriving the matrix equation of motion (1), the energy storing mechanism resulting from the initial stress is retained to include the effects due to internal or external pressures.

To avoid dimension dependence, the equations of motion are initially normalized by defining the following dimensionless parameters (White, 1986): $a^* = a/l$, $h^* = h/l$, $\mathbf{u}^* = \mathbf{u}/l$, p^*/E, and $t^* = \sqrt{E/\rho}\cdot t/l$ where E and ρ denote the Young's modulus and the density of the tube, respectively. Consequently, the equations are rewritten as

$$\{[L_L^*] + [L_P^*]\}\mathbf{u}^* = \mathbf{0}. \quad (5)$$

To neatly express the equations, the asterisks are removed hereafter. The two differential operators are of the forms

$$[L_L^*] = \begin{bmatrix} \left[K\frac{\partial^2}{\partial\xi^2} + \frac{K(1-\nu)}{2a^2}\frac{\partial^2}{\partial\theta^2} - h\frac{\partial^2}{\partial t^2}\right] & \frac{K(1+\nu)}{2a}\frac{\partial^2}{\partial\xi\partial\theta} & \frac{\nu K}{a}\frac{\partial}{\partial\xi} \\ & \left[\frac{1-\nu}{2}\left(K + \frac{D}{a^2}\right)\frac{\partial^2}{\partial\xi^2} + \left(\frac{D}{a^4} + \frac{K}{a^2}\right)\frac{\partial^2}{\partial\theta^2} - h\frac{\partial^2}{\partial t^2}\right] & \left[-\frac{D}{a^4}\frac{\partial^3}{\partial\theta^3} + \frac{K}{a^2}\frac{\partial}{\partial\theta} - \frac{D}{a^2}\frac{\partial^3}{\partial\xi^2\partial\theta}\right] \\ \text{sym.} & & \left[\frac{D}{a^4}\nabla^4 + \frac{K}{a^2} + h\frac{\partial^2}{\partial t^2}\right] \end{bmatrix} \quad (6)$$

and

$$[L_P^*] = \begin{bmatrix} \frac{p}{a}\frac{\partial^2}{\partial\theta^2} & 0 & 0 \\ & \left[\frac{p}{a}\frac{\partial^2}{\partial\theta^2} - \frac{p}{a}\right] & 2\frac{p}{a}\frac{\partial}{\partial\theta} \\ \text{sym.} & & \left[\frac{p}{a} - \frac{p}{a}\frac{\partial^2}{\partial\theta^2}\right] \end{bmatrix}. \quad (7)$$

EFFECTS OF INTERNAL FLOWS

Constant Internal Pressure

The simplest case of constant internal pressure is first discussed. The shell is further assumed to be simply supported at both ends, i.e., at $\xi = 0$, or 1,

$$u_z(\xi, \theta, t) = 0,$$
$$u_\theta(\xi, \theta, t) = 0,$$

$$M_x(\xi, \theta, t) = 0, \qquad N_x(\xi, \theta, t) = 0. \tag{8}$$

Here M_x and N_x denote the bending moment resultant and membrane force resultant, respectively. They are of the forms

$$M_x = D\left[-\frac{\partial^2 u_z}{\partial \xi^2} + \frac{\nu}{a^2}\left(\frac{\partial u_\theta}{\partial \theta} - \frac{\partial^2 u_z}{\partial \theta^2}\right)\right], \tag{9}$$

$$N_x = K\left[\frac{\partial u_x}{\partial \xi} + \frac{\nu}{a}\left(\frac{\partial u_\theta}{\partial \theta} + u_z\right)\right]. \tag{10}$$

Notably, in reality the tube may not be simply supported at the ends. However, Saito and Endo (1986) proved that the boundaries do not significantly change the dynamic characteristics of the shell as long as the tube is sufficiently slender. The tubes in the heat exchanger are in general relatively long; therefore, the assumption of simple supports is reasonable in this study.

The mode shapes of the cylindrical shell are shown to be of the forms (Huang and Hsu, 1990)

$$\begin{aligned} u_x &= A_x \cos m\pi\xi \cos n\theta \cos \omega^*_{mn} t, \\ u_\theta &= A_\theta \sin m\pi\xi \sin n\theta \cos \omega^*_{mn} t, \\ u_z &= A_z \sin m\pi\xi \cos n\theta \cos \omega^*_{mn} t, \end{aligned} \tag{11}$$

where the dimensionless frequency is defined as $\omega^*_{mn} = \sqrt{\rho/E}\, l\omega_{mn}$; ω_{mn} denotes the natural frequency associated with the (m, n) mode; m and n represent the longitudinal half-wave and the circumferential wave numbers, respectively; and A_x, A_θ, and A_z are undetermined amplitudes.

By substituting the expressions (11) into the equations of motion, a set of linear algebraic equations, in terms of the variables $\mathbf{A} = \{A_x, A_\theta, A_z\}^T$, can be obtained as follows:

$$\mathbf{\Delta A} = \mathbf{0}, \tag{12}$$

where

$$\mathbf{\Delta} = \begin{bmatrix} h(\omega^{*2}_{mn} - \hat{a}) & \hat{b} & \hat{c} \\ & h(\omega^{*2}_{mn} - \hat{d}) & -\hat{e} \\ \text{sym.} & & h(\omega^{*2}_{mn} - \hat{f}) \end{bmatrix}. \tag{13}$$

Table 1. Geometric and Material Parameters of the Shell

Density	$\rho = 8.75 \times 10^{-9}$ N s^2/mm^4
Length	$l = 300$ mm
Thickness	$h = 2$ mm
Mean radius	$a = 100$ mm
Poisson's ratio	$\nu = 0.34$
Young's modulus	$E = 11.5 \times 10^4$ N/mm^2

Here the defined parameters $\hat{a}, \ldots, \hat{f}$ are given in the Appendix. To yield nontrivial solutions, the determinant of $\mathbf{\Delta}$ should vanish. This yields the frequency equation of the cylindrical tube with internal constant pressure flow as

$$\omega^{*6}_{mn} + a_4\omega^{*4}_{mn} + a_2\omega^{*2}_{mn} + a_0 = 0, \tag{14}$$

where

$$\begin{aligned} a_4 &= -(\hat{a} + \hat{d} + \hat{f}), \\ a_2 &= (a\hat{f} + \hat{a}\hat{d} + \hat{d}\hat{f} - \hat{b}^2 - \hat{c}^2 - \hat{e}^2), \\ a_0 &= (\hat{a}\hat{e}^2 + \hat{d}\hat{c}^2 + \hat{f}\hat{b}^2 - \hat{a}\hat{d}\hat{f} - 2\hat{b}\hat{c}\hat{e}). \end{aligned} \tag{15}$$

Consequently, the amplitude ratios of the (m, n) mode can be obtained as

$$\frac{A_\theta}{A_x} = \frac{\begin{vmatrix} -\hat{b} & -\hat{e} \\ -\hat{c} & \omega^{*2}_{mni} - \hat{f} \end{vmatrix}}{\begin{vmatrix} \omega^{*2}_{mni} - \hat{d} & -\hat{e} \\ -\hat{e} & \omega^{*2}_{mni} - \hat{f} \end{vmatrix}} \quad \text{and} \qquad \frac{A_z}{A_x} = \frac{\begin{vmatrix} \omega^{*2}_{mni} - \hat{a} & -\hat{b} \\ -\hat{e} & -\hat{c} \end{vmatrix}}{\begin{vmatrix} \omega^{*2}_{mni} & -\hat{e} \\ -\hat{e} & \omega^{*2}_{mni} - \hat{f} \end{vmatrix}}. \tag{16}$$

Note that the third subscript $i = 1, 2, 3$ in Eq. (16) is designated for three different modes corresponding to the same (m, n) number. Usually, one assigns $\omega_{mn1} \le \omega_{mn2} \le \omega_{mn3}$. Physically, ω_{mn1} is the frequency associated with the mode where the bending vibration predominates. The other two frequencies are respectively associated with the modes where the torsional (circumferential) or the longitudinal vibration predominates. For developable surfaces like cylindrical tubes, the bending modes ($i = 1$) are generally of the lowest frequency and of the most significance.

Table 1 lists the material and geometric param-

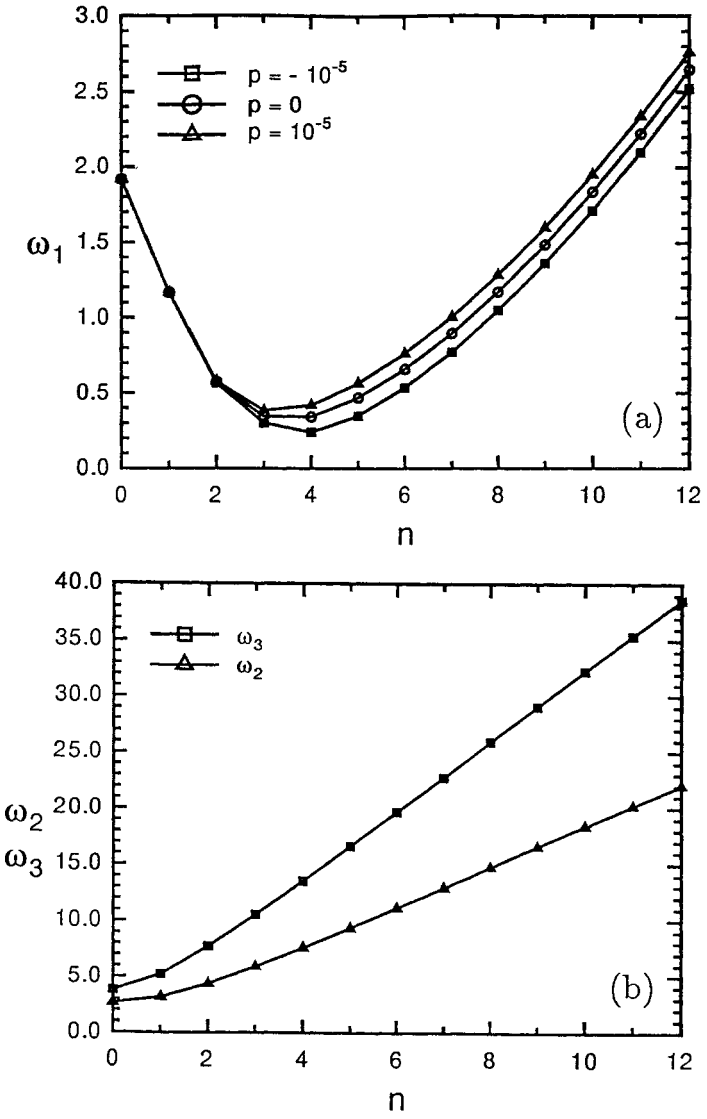

FIGURE 2 Natural frequencies, with $m = 1$, of the tube subjected to internal flow for (a) bending modes and (b) torsional and longitudinal modes.

eters of the illustrated shell for numerical examples shown hereafter. Figure 2 presents the natural frequencies of $m = 1$ for three different values of internal pressure. Figure 2(a) depicts the bending frequencies and Fig. 2(b) shows the higher two sets of frequencies. According to these figures, increasing internal pressure causes increasing bending frequencies of $n > 2$ modes. However, the pressure change does not influence the torsional and longitudinal natural frequencies, as shown in Fig. 2(b).

Figure 3 illustrates the variance of shell bending frequencies with the internal pressure for $m = 1$ and $n = 1$, 4, 7, and 10 modes. As this figure reveals, except for the $n = 1$ mode, the frequencies increase linearly with the internal pressure. The natural frequencies of $n = 1$ modes barely vary with the internal pressure. At these modes, such a slight variance is due to the tube's cross section remaining circular, similar to the situation at a rigid body mode. Consequently, the internal pressure becomes insignificant to these frequencies.

Periodic Internal Pressure

The internal flow can periodically fluctuate with respect to a constant pressure. The pulsation may originate from the pumping effect or others in

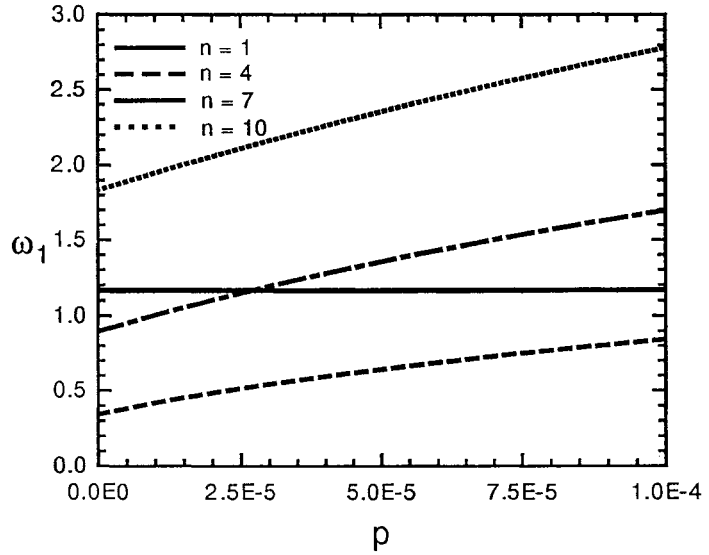

FIGURE 3 Bending natural frequencies, with $m = 1$, of the tube subjected to internal flow for variance of pressure values.

practice. This variation is, however, of smaller amplitude and lower frequency compared to the shell stress wave. Hence, it is reasonable to assume

$$p = p_0(1 + \varepsilon \cos \Omega t), \tag{17}$$

where p_0 is a constant pressure, the small parameter ε denotes the perturbation of flow pressure, and Ω is the pulsation frequency of the flow. Substituting (17) into the shell equations, one can obtain a relatively complicated parametric system. Exact solution is infeasible; hence, Galerkin's method is employed. We then select the trial set of comparison functions as

$$\begin{aligned} \phi_x(\xi, \theta) &= \cos m\pi\xi \cos n\theta, \\ \phi_\theta(\xi, \theta) &= \sin m\pi\xi \sin n\theta, \\ \phi_z(\xi, \theta) &= \sin m\pi\xi \cos n\theta, \end{aligned} \tag{18}$$

and assume

$$\mathbf{u} = \begin{Bmatrix} u_x \\ u_\theta \\ u_z \end{Bmatrix} = \begin{Bmatrix} \sum_{m=1}\sum_{n=1} A_{mn}(t)\phi_x(\xi, \theta) \\ \sum_{m=1}\sum_{n=1} B_{mn}(t)\phi_\theta(\xi, \theta) \\ \sum_{m=1}\sum_{n=1} C_{mn}(t)\phi_z(\xi, \theta) \end{Bmatrix}, \tag{19}$$

in which A_{mn}, B_{mn}, and C_{mn} are referred to as generalized coordinates.

Substituting the displacement functions into the equations of motion yields a set of Mathieu's equations for each (m, n) combination expressed as

$$\ddot{\mathbf{x}} + \{[K_A] + 2\varepsilon[K_B]\cos \Omega t\}\mathbf{x} = 0, \tag{20}$$

with

$$\mathbf{x} = \{A_{mn}, B_{mn}, C_{mn}\}^T, \tag{21}$$

$$[K_A] = \begin{bmatrix} \hat{a} & -\hat{b} & -\hat{c} \\ -\hat{b} & \hat{d} & \hat{e} \\ -\hat{c} & \hat{e} & \hat{f} \end{bmatrix} \quad \text{and}$$

$$[K_B] = \begin{bmatrix} \hat{g} & 0 & 0 \\ 0 & \hat{h} & \hat{i} \\ 0 & \hat{i} & \hat{h} \end{bmatrix}, \tag{22}$$

in which parameters $\hat{g}$, $\hat{h}$, and $\hat{i}$ are listed in the Appendix.

To simplify the solution process, a linear transform is introduced, i.e., $\mathbf{x} = [P]\mathbf{v}$ where $[P]^{-1}[K_A][P]$ forms a Jordan canonical form. After transformation, Mathieu's equation, Eq. (20) becomes

$$\ddot{\mathbf{v}} + \begin{bmatrix} \omega_1^2 & 0 & 0 \\ 0 & \omega_2^2 & 0 \\ 0 & 0 & \omega_3^2 \end{bmatrix} \mathbf{v} + 2\varepsilon \cos \Omega t\,[G]\mathbf{v} = \mathbf{0}, \tag{23}$$

where $[G] = [P]^{-1}[K_B][P]$ and ω_i is the natural frequency of the tube at $p = p_0$. The above equation can be further expanded into a component form as

$$\ddot{v}_i + \omega_i^2 v_i + 2\varepsilon \cos \Omega t \sum_{j=1}^{3} g_{ij} v_j = 0, \tag{24}$$

with $i = 1, 2, 3$ for each set of (m, n).

Equation (24) presents a coupled parametrically excited system, and the method of multiple scales can be applied for the solution. The method involves expressing the system response in terms of a series of the small perturbation ε (Nayfeh and Mook, 1979) with

$$\begin{aligned} v_i(\varepsilon, t) = {} & v_{i0}(T_0, T_1, T_2, \ldots) \\ & + \varepsilon v_{i1}(T_0, T_1, T_2, \ldots) \\ & + \varepsilon^2 v_{i2}(T_0, T_1, T_2, \ldots) + \cdots \end{aligned} \tag{25}$$

in which $T_n = \varepsilon^n t$ denotes different time scales. The time derivatives are then expressed as

$$\frac{d}{dt} = D_0 + \varepsilon D_1 + \varepsilon^2 D_2 + \cdots \tag{26}$$

$$\frac{d^2}{dt^2} = D_0^2 + 2\varepsilon D_0 D_1 + \varepsilon^2 (2 D_0 D_2 + D_1^2) + \cdots \tag{27}$$

$$\vdots$$

by denoting $D_n = \partial / \partial T_n$. Treating each time scale as an independent variable, substituting Eq. (25) to (27) into Eq. (24), and rearranging it in an ascending order of ε, produces

$$D_0^2 v_{i0} + \omega_i^2 v_{i0} = 0, \tag{28}$$

$$D_0^2 v_{i1} + \omega_i^2 v_{i1} = -2 D_0 D_1 v_{i0} - \sum_{j=1}^{3} g_{ij} v_{j0} (e^{i\Omega T_0} + \text{CC}), \tag{29}$$

$$D_0^2 v_{i2} + \omega_i^2 v_{i2} = -2 D_0 D_1 v_{i1} - 2 D_0 D_2 v_{i0} - D_1^2 v_{i0} - \sum_{j=1}^{3} g_{ij} v_{i1} (e^{i\Omega T_0} + \text{CC}) \tag{30}$$

$$\vdots$$

where $i = 1, 2, 3$, and CC represents the complex conjugate of the preceding terms. The solution of Eq. (28) appears to be in the form of

$$v_{i0} = A_i(T_1, T_2) e^{i\omega_i T_0} + \text{CC}. \tag{31}$$

By substituting (31) into Eq. (29), one can obtain

$$D_0^2 v_{i1} + \omega_i^2 v_{i1} = -2 i \omega_i D_1 A_i e^{i\omega_i T_0} - \sum_{j=1}^{3} g_{ij} A_j [e^{i(\omega_i + \Omega) T_0} + e^{i(\omega_i - \Omega) T_0}] + \text{CC} \tag{32}$$

with $i = 1, 2, 3$. Note that the undetermined complex constant A_i in Eq. (31) can be found by eliminating the secular terms in Eq. (32). Eliminating these divergent terms, however, depends on the value of Ω and cases are discussed in the following:

1. Ω far away $\omega_p \pm \omega_q$, $p, q = 1, 2, 3$: For this case, we can obtain

$$D_1 A_i = 0. \tag{33}$$

The above equation implies that A_i can be treated as a constant and no instability is found.

2. Ω close to $\omega_p + \omega_q$: This is called the combination resonance of the summed type. A detuning parameter σ is introduced as

$$\Omega = \omega_p + \omega_q + \varepsilon\sigma. \tag{34}$$

Consequently, we have

$$(\Omega - \omega_p) T_0 = \omega_q T_0 + \sigma \varepsilon T_0 = \omega_q T_0 + \sigma T_1, \tag{35}$$

$$(\Omega - \omega_q) T_0 = \omega_p T_0 + \sigma T_1, \tag{36}$$

in which g_{pq} and g_{qp} are complicated functions of all systems parameters (Hsu, 1992). Substituting the above two equations into Eq. (32) and rearranging the terms, produces the following equations:

$$2 i \omega_p D_1 A_p + g_{pq} \tilde{A} q e^{i\sigma T_1} = 0, \tag{37}$$

$$2 i \omega_q D_1 A_q + g_{qp} \tilde{A}_p e^{i\sigma T_1} = 0, \tag{38}$$

by eliminating the secular terms in the right-hand side of Eq. (32). In the above equations the tilde notation represents the complex conjugate of the complex variable, and g_{pq} and g_{gp} are complicated functions of all system parameters (Hsu, 1992). The solution to Eqs. (37) and (38) appears to be

$$A_p = a_p e^{-i\lambda T_1}, \tag{39}$$

$$A_q = a_q e^{i(\tilde{\lambda} + \sigma) T_1}, \tag{40}$$

where a_p and a_q are complex functions in T_2, $\lambda = -(1/2)[\sigma \pm (\sigma^2 - \Lambda_{pq})^{1/2}]$, and $\Lambda_{pq} = g_{pq}g_{pq}/\omega_p\omega_q$. Thus, A_p and A_q are bounded if and only if

$$\sigma^2 \geq \Lambda_{pq}. \tag{41}$$

This situation is automatically satisfied if g_{pq} and g_{qp} are of opposite signs. The response is hence bounded. If g_{pq} and g_{qp} are of the same sign, one can determine the stability boundaries in the following form:

$$\Omega = \omega_p + \omega_q \pm \varepsilon \left[\frac{g_{pq}g_{qp}}{\omega_p\omega_q}\right]^{1/2} + O(\varepsilon^2). \tag{42}$$

This equation is actually two curves on the ε–Ω plane and the area enclosed by these curves is the unstable region. The ε–Ω plane is then divided into several stable regions and unstable regions. In the unstable region, the response is divergent and subsequently causes instability.

3. Ω close to $\omega_p - \omega_q$: This case is referred to as combination resonance of a difference type. The equations of the stability boundaries can be derived in the same manner as described previously except changing the sign of ω_q (Hsu, 1992). Instability occurs only if g_{pq} and g_{qp} are of opposite signs. However, instability does not exist for the illustrated system because $[G]$ is symmetric.

In the following, the stability of different (m, n) modes is discussed from the expression of Eq. (42). Figures 4 and 5 show the stability boundaries associated with $m = 1$ and different n for $p_0 = 10^{-4}$ and $p_0 = 10^{-3}$, respectively. Six resonant frequencies, with respect to each combination of (m, n), need to be taken into account. They are Ω close to $2\omega_1$, $\omega_1 + \omega_2$, $\omega_1 + \omega_3$, $2\omega_2$, $\omega_2 + \omega_3$, or $2\omega_3$ from left to right in these figures. Each combination consists of two curves that enclose an unstable region. The regions with the marked sign S are the stable ones and those in between are unstable regions. These figures show that all stability boundaries are actually straight lines. This fact is attributed to merely the solution of order ε^1 being solved in the method of multiple scales.

Figure 4 for $p_0 = 10^{-4}$ indicates that the unstable regions near $2\omega_2$ and $\omega_1 + \omega_3$ are too close to distinguish. The unstable region for $n = 7$ becomes wider at $2\omega_1$, compared to that for $n = 1$. For a higher internal pressure and $n = 1$, the unstable regions corresponding to higher resonant frequencies are larger than those due to smaller internal pressure [Fig. 5(a)]. Regarding the unstable regions for higher modes ($n = 7$), the areas of the unstable regions near lower resonant frequencies, particularly $2\omega_1$, also apparently increase. We can thus conclude that the instability motion of the tube is more likely to occur at higher modes.

EFFECTS OF EXTERNAL CROSS FLOWS

Under the action of the external flows, the pressure distribution on the tube is generally not uniform but is a function of θ. Hence, the pressure is expressed as $p = p(\theta)$. However, this function is difficult to solve analytically. Instead, it was determined from the interpolation of experimental measurements or numerical calculations (Dhaubhadel et al., 1987; Žukauskas et al., 1988). In the present research, the existing data in the available literature (Žukauskas et al., 1988) was adopted directly. To analytically examine the dynamic behavior of tubes, the numerical data curves were fitted and transformed to Fourier series. Analytical expressions of pressure functions were hence obtained.

Steady External Cross Flows

For this case, the pressure distribution is assumed to vary with θ but not time. The displacement functions, for some specific m, can be expressed as

$$\begin{aligned} u_x &= \cos m\pi\xi\Phi_x(\theta)e^{i\omega t}, \\ u_\theta &= \sin m\pi\xi\Phi_\theta(\theta)e^{i\omega t}, \\ u_z &= \sin m\pi\xi\Phi_z(\theta)e^{i\omega t}, \end{aligned} \tag{43}$$

where $\Phi_j(\theta)$, $j = x, \theta, z$ are shape functions in θ. These shape functions can be further expressed in the form of the Fourier series as

$$\begin{aligned} \Phi_x &= \textstyle\sum_{n=1}^{k} a_n \cos n\theta, \\ \Phi_\theta &= \textstyle\sum_{n=1}^{k} b_n \sin n\theta, \\ \Phi_z &= \textstyle\sum_{n=1}^{k} c_n \cos n\theta. \end{aligned} \tag{44}$$

This assumption is based on the periodicity, in circumferential direction, of the pressures and the resulting displacements due to the external cross flow. In the above expression, a_n, b_n, and c_n are the undetermined constants for the specific m. By

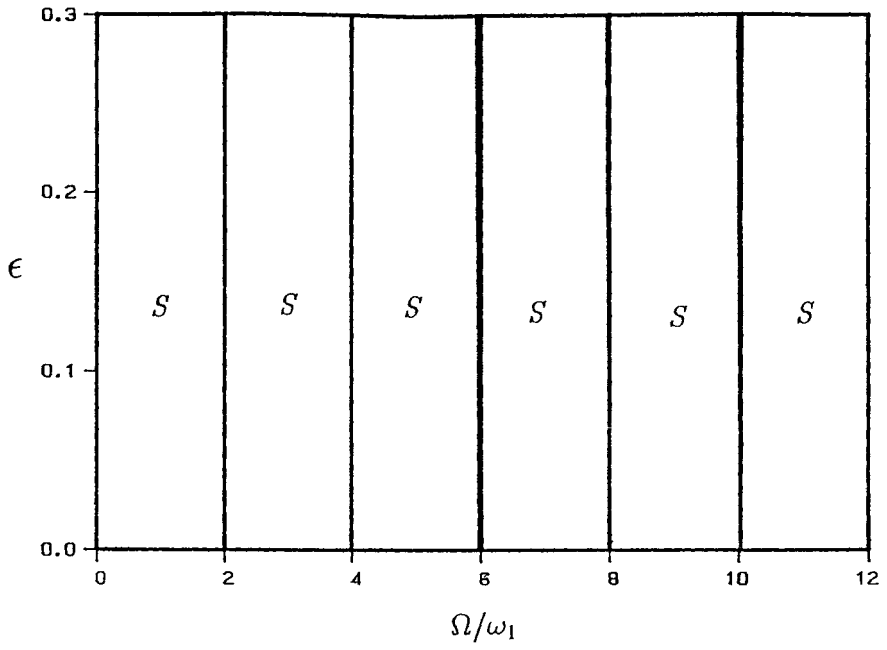

(a) n = 1

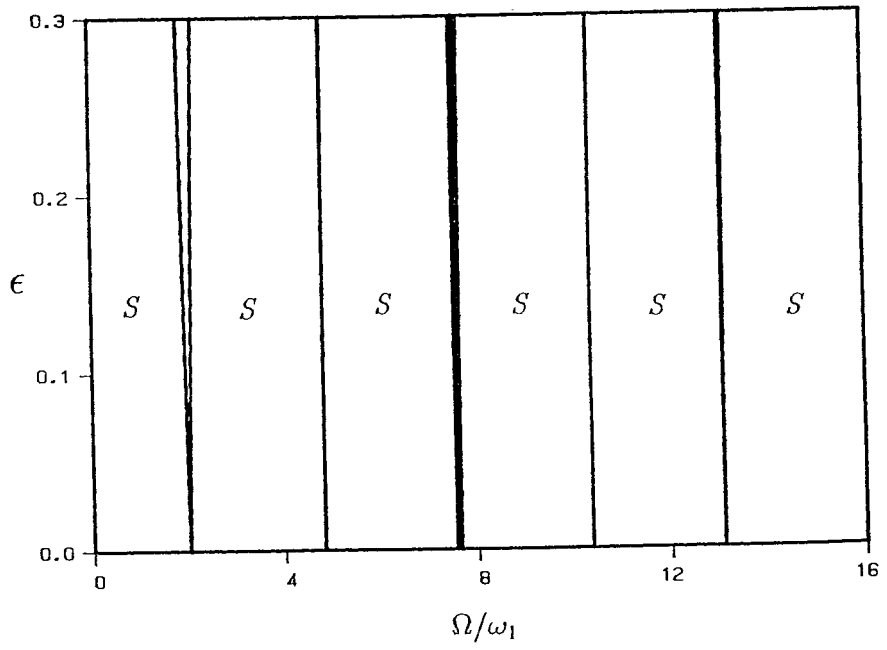

(b) n = 7

FIGURE 4 Stability diagrams of the tube subjected to periodic internal flow for $p_0 = 10^{-4}$, $m = 1$, and (a) $n = 1$ and (b) $n = 7$.

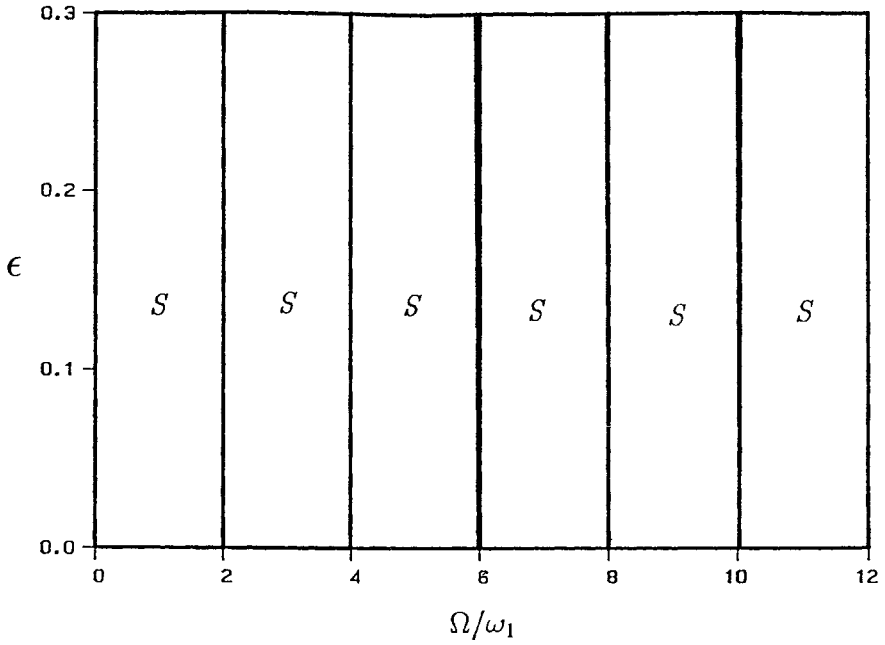

(a) n = 1

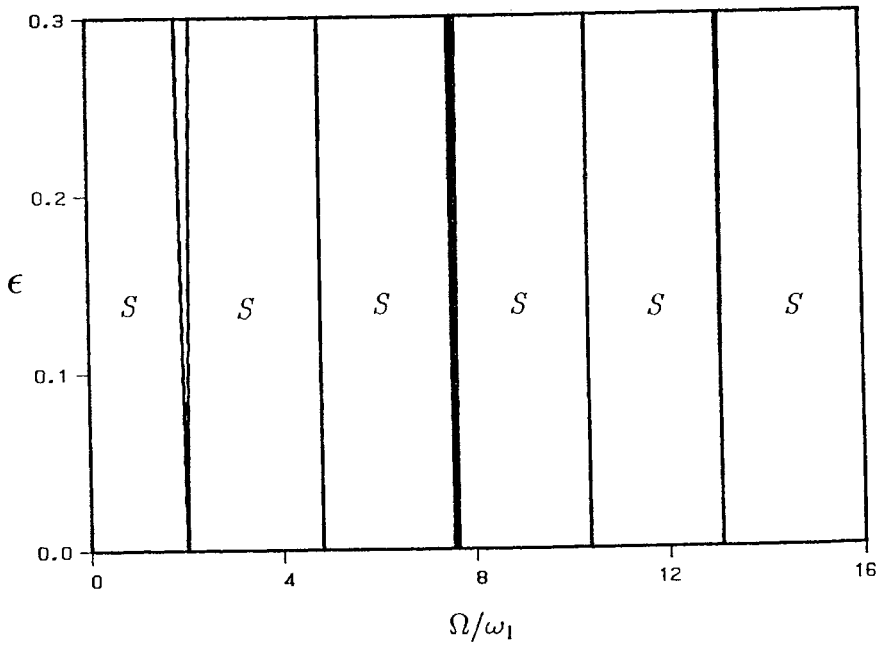

(b) n = 7

FIGURE 5 Stability diagrams of the tube subjected to periodic internal flow for $p_0 = 10^{-3}$, $m = 1$, and (a) $n = 1$ and (b) $n = 7$.

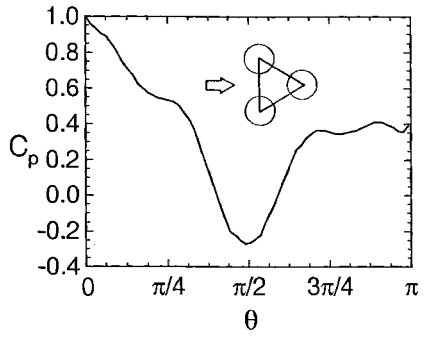

FIGURE 6 Distribution of pressure coefficient with tube angles for a staggered tube bundle.

employing Galerkin's method, the equations of motion of (5) can be written as the following eigenvalue problem:

$$\omega^2[M]\mathbf{a} = [K]\mathbf{a}, \tag{45}$$

with $\mathbf{a} = \{a_1, a_2, \ldots, a_k, b_1, b_2, \ldots, b_k, c_1, c_2, \ldots, c_k\}^T$, and $[M]$ and $[K]$ are the inertia matrix and the stiffness matrix, respectively (Hsu, 1992).

Equation (45) is an eigenvalue problem of order $3k$, provided an m value is given. Hence, $3k$ natural frequencies correspond to the external pressure $p(\theta)$. The eigenvectors can also be solved correspondingly.

Figure 6 illustrates the pressure coefficient C_p as a function of θ for a staggered tube bundle system with a Reynold's number (Re) = 10^6. The pitch to diameter ratio of the shown system is 1.25. The data used in this article were digested directly from the reference (Žukauskas et al., 1988). Notably, the above data were selected from tubes in the deep rows, and the $\theta = 0$ point was marked as the point where the flow was first acted upon. Moreover, the figure merely shows the pressure coefficient from 0 to π. The pressure coefficient in π to 2π is assumed to be symmetric. One can then use the curve fitting technique to express the curve in an analytical Fourier series form of

$$C_p(\theta) = \alpha_0 + \sum_{j=1}^{5} (\alpha_j \cos j\theta + \beta_j \sin j\theta), \tag{46}$$

where a total of 11 terms are selected according to the numerical calculation (Hsu, 1992). In addition, the dimensionless pressure coefficient $C_p(\theta)$ is related to the dimensionless pressure function $p(\theta)$ by the following (Žukauskas et al., 1988):

$$C_p(\theta) = 1 - \frac{\frac{1}{2}\rho_f U^2 - Ep(\theta)}{\frac{1}{2}\rho_f \overline{U}^2}, \tag{47}$$

in which ρ_f is fluid density, U is flow velocity, $\overline{U}$ is the average flow velocity between two neighboring tubes, and usually we have $U < \overline{U}$. The pressure function is then solved from Eq. (47) and is substituted into the equations of motion (5). After per-

Table 2. Natural Frequencies of Staggered Tube Bundle

n	$p = 0, m = 1$	$p = p(\theta), m = 1$	$p = 0, m = 2$	$p = p(\theta), m = 2$
		Bending Frequency, ω_1		
1	1.1669	1.1668	2.2329	2.2317
2	0.5743	0.5754	1.4495	1.4483
3	0.3454	0.3509	0.9565	0.9560
4	0.3418	0.3576	0.7132	0.7167
5	0.4690	0.4880	0.6731	0.6819
		Torsional Frequency, ω_2		
1	3.1602	3.1602	4.5509	4.5510
2	4.3587	4.3587	5.6134	5.6136
3	5.9214	5.9215	6.9123	6.9125
4	7.6265	7.6265	8.4044	8.4047
5	9.3890	9.3890	10.0168	10.0170
		Longitudinal Frequency, ω_3		
1	5.2160	5.2162	7.5759	7.5759
2	7.7356	7.7360	9.4920	9.4921
3	10.5681	10.5686	11.9469	11.9472
4	13.5424	13.5430	14.6664	14.6669
5	16.5906	16.5914	17.5335	17.5341

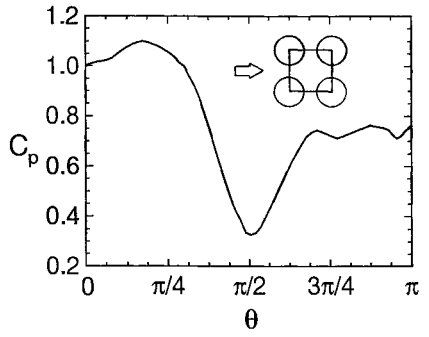

FIGURE 7 Distribution of pressure coefficient with tube angles for an in-line tube bundle.

forming Galerkin's method, the eigenvalue problem (45) is resolved.

The fluid encountered in this study is water. Table 2 lists the solved natural frequencies for $m = 1, 2$ in which the frequencies associated with no external pressure are also listed for comparison. As this table reveals, the external cross flows barely change the higher set of frequencies, i.e., ω_2, ω_3, because these frequencies correspond to the torsional and longitudinal modes. On the other hand, the external cross flow can alter the bending frequencies. Some frequencies are lifted up, but some drift slightly down. Such an occurrence is caused by irregularity of pressure function.

Figure 7 displays the pressure coefficients of an in-line tube bundle system (1.25 × 1.25). The data are again obtained from the book by Žukauskas et al. (1988). A similar process is performed and the results are listed in Table 3 for the first set of natural frequencies. Although not given in the table, we can conclude that the external steady flow merely affects the values of bending frequencies of the in-line tube bundle.

Periodically Varying Flows

Tube dynamics, particularly instability conditions, due to slightly perturbed flows is investigated. Assume that the real external pressure $\bar{p}$ is a slight perturbation about the pressure $p(\theta)$ as the following:

$$\bar{p}(\theta, t) = p(\theta)(1 + \varepsilon \cos \bar{\Omega} t), \tag{48}$$

in which ε is a small disturbance and $\bar{\Omega}$ is the perturbed frequency.

Similar to the process of analyzing the internal flow, Galerkin's method is employed herein. Consequently, a Mathieu's equation in the matrix form for each (m, n) combination is obtained as

$$\ddot{\mathbf{x}} + \{[K_a] + 2\varepsilon[K_b]\cos \bar{\Omega} t\}\mathbf{x} = 0, \tag{49}$$

with

$$\mathbf{x} = \{\bar{A}_{mn}, \bar{B}_{mn}, \bar{C}_{mn}\}^T, \tag{50}$$

$$[K_a] = \begin{bmatrix} \bar{a} & -\hat{b} & -\hat{c} \\ -\hat{b} & \bar{d} & \bar{e}_1 \\ -\hat{c} & \bar{e}_2 & \bar{f} \end{bmatrix} \quad \text{and}$$

$$[K_b] = \begin{bmatrix} \bar{g} & 0 & 0 \\ 0 & \bar{h}_1 & \bar{i}_1 \\ 0 & \bar{i}_2 & \bar{h}_2 \end{bmatrix}. \tag{51}$$

The defined parameters are given in the Appendix. The similar process in internal flow analysis is next performed, and stability boundaries in the ε–Ω plane are obtained accordingly. It seems that the instabilities occur more easily for the tube subjected to the internal flow than for the external cross flow. From the previous results for the internal flow, more instabilities were found at higher modes than at lower modes. Our results thus concentrate on the stability at vibrating modes with higher natural frequencies. Figure 8 depicts the stability diagram for $m = 5$ and $n = 7$ of a staggered tube bundle system. The plane is again divided into stable and six unstable regions. As this figure demonstrates, the unstable regions are very narrow and become single lines. Instability can occur

Table 3. Bending Natural Frequencies of In-Line Tube Bundle

	Bending Frequency, ω_1			
n	$p = 0, m = 1$	$p = p(\theta), m = 1$	$p = 0, m = 2$	$p = p(\theta), m = 2$
1	1.1669	1.1668	2.2329	2.2318
2	0.5743	0.5741	1.4495	1.4477
3	0.3454	0.3455	0.9565	0.9536
4	0.3418	0.3426	0.7132	0.7096
5	0.4690	0.4702	0.6731	0.6695

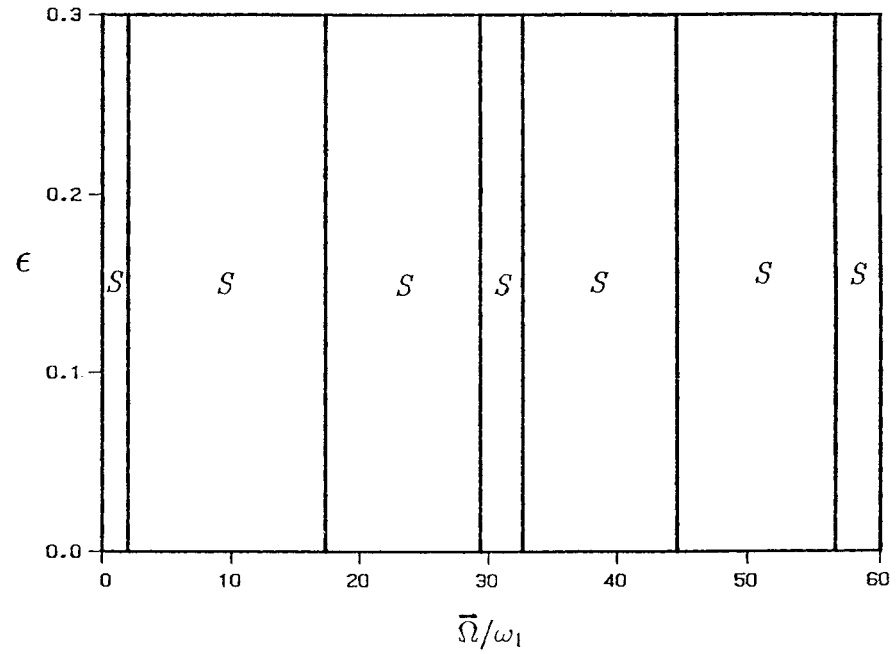

FIGURE 8 Stability diagram of the tube subjected to periodic external flow for $m = 5$ and $n = 7$.

only when the perturbed frequency $\bar{\Omega}$ is exactly equal to one of the six unstable resonant frequencies. The presented method can be used to analyze the tube's dynamic response and its stability, provided that the pressure distribution function $p(\theta)$ is obtained by analytical, numerical, or experimental techniques. Notably, the stability of the tube vibration depends heavily on the type of tube bundle system.

CONCLUDING REMARKS

This study presents a method for examining the free vibration and the dynamic instability of cylindrical tubes subjected to internal flows or external cross flows. From the numerical results presented herein, we can conclude the following:

1. For the case of the internal flow with a constant pressure, increasing the pressure caused initial stress in the tube, and subsequently raised the bending natural frequencies of the $n > 1$ modes. However, the vibration at $n = 1$ modes, which are similar to a rigid body mode in the circumferential direction, seemed unaffected by the internal pressure. The internal pressure was also found to be insignificant with respect to the torsional and longitudinal modes of the tubes.
2. For the periodic internal flow, the governing equations became parametric ones. The stability diagrams were established using the method of multiple scales. The unstable regions became wider by increasing perturbing magnitude. In addition, instability would most likely occur at higher n numbers.
3. If the tube is subjected to an external cross flow, this study provides an analytical approach for this type of problem. The pressure distribution from experiment data was written analytically as Fourier series. Numerical simulation demonstrates that external cross flows did not cause severe stability problems based on the current model.

Part of this work was sponsored by the National Science Council, ROC (Grant NSC 80-0401-E008-01) and the Institute of Nuclear Energy Research, ROC. Their support is gratefully acknowledged.

APPENDIX

Defined shell parameters:

$$\hat{a} = \left[K(m\pi)^2 + \frac{K}{2}(1-\nu)\left(\frac{n}{a}\right)^2 + \frac{p}{a}n^2 \right] \Big/ h$$

$$\hat{b} = \frac{1+\nu}{2ah} Kmn\pi$$

$$\hat{c} = \frac{\nu K}{ah} m\pi$$

$$\hat{d} = \left[n^2 \left(\frac{D}{a^4} + \frac{K}{a^2} + \frac{p}{a} \right) + \frac{1-\nu}{2} \left(K + \frac{D}{a^2} \right) (m\pi)^2 + \frac{p}{a} \right] \Big/ h$$

$$\hat{e} = n \left[n^2 \frac{D}{a^4} + \frac{K}{a^2} + 2\frac{p}{a} + \frac{D}{a^2} (m\pi)^2 \right] \Big/ h$$

$$\hat{f} = \left[n^4 \frac{D}{a^4} + \frac{K}{a^2} + \frac{p}{a} n^2 + 2\frac{n^2 D}{a^2} (m\pi)^2 + D(m\pi)^4 + \frac{p}{a} \right] \Big/ h$$

$$\hat{g} = \frac{n^2 p_0}{2ah}$$

$$\hat{h} = \frac{(n^2+1)p_0}{2ah}$$

$$\hat{i} = \frac{np_0}{ah}$$

$$\bar{a} = \left[K(m\pi)^2 + \frac{K}{2}(1-\nu) \left(\frac{n}{a} \right)^2 + \frac{p_1}{a} n^2 \right] \Big/ h$$

$$\bar{d} = \left[n^2 \left(\frac{D}{a^4} + \frac{K}{a^2} + \frac{p_2}{a} \right) + \frac{1-\nu}{2} \left(K + \frac{D}{a^2} \right) (m\pi)^2 + \frac{p_2}{a} \right] \Big/ h$$

$$\bar{e}_1 = n \left[n^2 \frac{D}{a^4} + \frac{K}{a^2} + 2\frac{p_2}{a} + \frac{D}{a^2} (m\pi)^2 \right] \Big/ h$$

$$\bar{e}_2 = n \left[n^2 \frac{D}{a^4} + \frac{K}{a^2} + 2\frac{p_3}{a} + \frac{D}{a^2} (m\pi)^2 \right] \Big/ h$$

$$\bar{f} = \left[n^4 \frac{D}{a^4} + \frac{K}{a^2} + \frac{p_3}{a} n^2 + 2\frac{n^2 D}{a^2} (m\pi)^2 + D(m\pi)^4 + \frac{p_3}{a} \right] \Big/ h$$

$$\bar{g} = \frac{n^2 p_1}{2ah}$$

$$\bar{h}_1 = \frac{(n^2+1)p_2}{2ah}$$

$$\bar{h}_2 = \frac{(n^2+1)p_3}{2ah}$$

$$\bar{i}_1 = \frac{np_2}{ah}$$

$$\bar{i}_2 = \frac{np_3}{ah}$$

where

$$p_1 = \frac{\Pi}{4} \int_0^\pi \int_0^1 \cos^2 m\pi\xi \cos^2 n\theta p(\theta) d\xi d\theta$$

$$p_2 = \frac{\Pi}{4} \int_0^\pi \int_0^1 \sin^2 m\pi\xi \sin^2 n\theta p(\theta) d\xi d\theta$$

$$p_3 = \frac{\Pi}{4} \int_0^\pi \int_0^1 \sin^2 m\pi\xi \cos^2 n\theta p(\theta) d\xi d\theta$$

REFERENCES

Blevins, R. B., 1977, *Flow-Induced Vibration,* Van Nostrand Reinhold, New York.

Chen, S. S., 1987, *Flow-Induced Vibration of Circular Cylindrical Structures,* Hemisphere, New York.

Dhaubhadel, M. N., Reddy, J. N., and Telionis, D. P., 1987, "Finite-Element Analysis of Fluid Flow and Heat Transfer for Staggered Bundles of Cylinders in Cross Flow," *International Journal for Numerical Methods in Fluids,* Vol. 7, pp. 1325–1342.

Hsu, C. S., 1992, "Dynamics of Tubes Subjected to Internal or External Cross Flows," MS. Thesis, National Central University, ROC.

Huang, S.C., and Hsu, B. S., 1990, "Resonant Phenomena of a Rotating Cylindrical Shell Subjected to a Harmonic Moving Load," *Journal of Sound and Vibration,* Vol. 132, pp. 215–228.

Leissa, A. W., 1973, *Vibration of Shells,* NASA SP-288, NASA, Washington, DC.

Nayfeh, A. H., and Mook, D. T., 1979, *Nonlinear Oscillations,* Wiley, New York.

Saito, T., and Endo, M., 1986, "The Vibration of Rotating Cylindrical Shells," *Bulletin of Japan Society of Mechanical Engineers,* Vol. 29, pp. 3505–3509.

Soedel, W., 1981, *Vibrations of Shells and Plates,* Dekker, New York.

Weaver, D. S., and Unny, T. E., 1973, "On the Dynamics

Stability of Fluid-Conveying Pipes," ASME *Journal of Applied Mechanics,* Vol. 40, pp. 48–52.

White, F. M., 1986, *Fluid Mechanics,* McGraw–Hill, New York.

Yao, J. C., 1963, "Dynamic Stability of Cylindrical Shells Under Static and Periodic Axial and Radial Loads," AIAA *Journal,* Vol. 1, pp. 1391–1396.

Žukauskas, A., Ulinskas, R., Katinas, V., and Karni, J., 1988, *Fluid Dynamics and Flow-Induced Vibrations of Tube Banks,* Hemisphere, New York.